ЖЭТФ/JETP, 2026, том 170, вып. 1 (7), стр. 17–31

IMPROVED TREATMENT OF RELATIVISTIC EFFECTS IN THE LINEAR AUGMENTED PLANE WAVE METHOD

A. V. Nikolaev [a*], ***U. N. Kurelchuk*** [b], ***E. V. Tkalya*** [b,c,d,e]

[a] *Skobeltsyn Institute of Nuclear Physics, Lomonosov Moscow State University 119234, Moscow, Russia*

[b] *National Research Nuclear University MEPhI 115409, Moscow, Russia*

[c] *P. N. Lebedev Physical Institute of the Russian Academy of Sciences 119991, Moscow, Russia*

[d] *Nuclear Safety Institute of the Russian Academy of Sciences 115191, Moscow, Russia*

[e] *Institute of Nuclear and Radiation Physics, Russian Federal Nuclear Center-VNIIEF 607188, Nizhny Novgorod region, Russia*

Received March 25, 2026,
revised version April 23, 2026
Accepted for publication May 18, 2026

We critically review the methodology for relativistic effects in the linear augmented plane wave method (LAPW) for solids and offer a few ways to account them more accurately. (1) We introduce new radial (Bloch-type) basis functions, based on two actual radial solutions of the Dirac equation for $j = l - 1/2$ and $j = l + 1/2$ states. This treatment differs from the canonical one, where for the basis function an effective differential equation is used. For the $6p$ semicore states of actinides the new basis function gets weight of the $6p_{1/2}$ component and can describe the $6p$ density adequately even without the $p_{1/2}$ local function. (2) We find that canonical matrix element expressions for the spherically symmetric potential are implicitly based on non-relativistic radial wave functions, which should be corrected. (3) In the canonical treatment the full spin-orbit (SO) energy splitting (in doubled basis set) of two $6p$ subbands is always overestimated. To reduce this value we suggest using the SO coupling constants $\zeta(p)$, $\dot{\zeta}(p)$, $\ddot{\zeta}(p)$, calculated with the $6p_{3/2}$ radial component. We apply the new treatment to solid Ac, Th, ThO_2, and UO_2, and discuss how new treatment affects the equilibrium lattice constants and bulk modulus. In the full treatment of SO coupling, UO_2 turns out to be a semimetal. For actinium a considerable overestimation of its lattice constant is observed.

Keywords: *ab initio* band structure calculations, relativistic effects, LAPW, spin-orbit coupling, thorium, actinium, ThO_2, UO_2

DOI: 10.31857/S0044451026070022

1. INTRODUCTION

Band structure calculations have become a powerful tool for studying complex materials, proving effective for many solids and capable of predicting their properties. The accuracy of such calculations is improving every year, and the demand for even greater accuracy and throughput is constantly growing. As shown in benchmark calculations [1], various methods for calculating band structures generally yield identical or similar final results (e. g., equilibrium lattice constants, bulk moduli, etc.). However, there is a class of materials for which the description of solids is less certain and presents difficulties. Such materials include, in particular, the heavy elements — actinides, located at the end of the Mendeleev Periodic Table, which have eighty or more core-shell electrons subject to relativistic effects. Several successful studies of the band struc-

* E-mail: nikolaev@sinp.msu.ru

ture of actinides have been published. The first studies were based on the linear muffin-tin method (LMTO) [2–5], followed by studies [6, 7] conducted using the full-potential linear augmented plane wave (FLAPW) method [8–11], considered one of the most accurate methods for determining the band structure. An additional complication arises from the fact that electrons belonging to the incompletely filled $5f$ shell of actinides exhibit a competition between itineracy and localization [12, 13]. This competition can lead to nontrivial magnetic and other correlation effects [14–18].

The canonical FLAPW approach uses the so-called scalar relativistic approach, based on the work of Koelling and Harmon in [19] (KH), and MacDonald, Pickett, and Koelling in Ref. [20]. (We will discuss this in detail below in Sec. 2.1.) Further developments have suggested enriching the FLAPW basis set with local atomic functions [21, 22], which can be fully relativistic, i. e., taken from the solution of the radial Dirac equation.

In Ref. [21] the relativistic $p_{1/2}$ local orbitals were added in the second variation step of the FLAPW calculation of elemental thorium, significantly improving the stability and accuracy of the band structure calculations. Note that the FLAPW method often uses two variational procedures as a time-saving computational scheme for taking into account spin-orbit (SO) coupling. In the first step only the scalar relativistic part of the Hamiltonian is diagonalized, whereas in the second variation step the SO coupling matrix is constructed and then diagonalized in a smaller basis set, consisting of a limited number of low lying eigenfunctions obtained on the first step and additional local atomic orbitals [21, 22]. In Ref. [21] only the $p_{1/2}$ relativistic atomic functions were used, while in Ref. [22] the method was extended to include other local relativistic functions and their combinations. The proposed corrections [21, 22] through the relativistic local orbitals in the second variation step being effective in practice, are based on the idea to increase the convergence and effectiveness of the basis set. They do not improve the relativistic characteristics of canonical LAPW (i. e., Bloch-like) band functions. In addition, the second variation step performed on a small number of secondary basis functions (which is usually considerably smaller the full basis set) can be considered as a perturbative treatment of the spin-orbit coupling [6].

The aim of this study is to improve the accuracy of accounting for relativistic effects within the full electron potential LAPW method by eliminating uncontrolled theoretical approximations and implicitly using non-relativistic relations. For that purpose (i) we introduce new basis functions, obtained from two independent solutions of the Dirac equation. In modern LAPW method one deals with two types of basis functions: Bloch-like LAPW basis functions and the atomic-like local orbitals (LO), which can be chosen to be fully relativistic (as, e. g., the $p_{1/2}$ mentioned earlier [21, 22]). In our work the new type of radial basis functions concerns the Bloch-type LAPW basis functions. We do not consider here the choice of local orbitals, which is a separate problem [11,23,24]. Further, (ii) we reconsider the matrix elements of the method, explicitly avoiding the use of hidden non-relativistic relations; (iii) we correct the calculation of the spin-orbit (SO) coupling constant for $6p$ semicore states, based on the comparison the energy splittings between $6p_{1/2}$ and $6p_{3/2}$ components. In the present study we do not apply the second variation procedure for the SO-coupling. We use the direct treatment of the SO coupling in the full LAPW basis set thereby avoiding the approximations associated with the second variation step [10]. These effects are considered and discussed in Sec. 2.1, Sec. 2.2, and Sec. 2.3, correspondingly. In Sec. 3 we briefly review the results of our calculations for Ac, Th, ThO_2, and UO_2, and finally in Sec. 4 we discuss main conclusions and findings of our work. In our study we use various variants of the DFT functionals (see Sec. 3 below), which allows us to test the accuracy of the calculations.

2. METHOD

In the LAPW method [8–10], widely used for studies of bulk materials, the space is partitioned in the region inside the nonoverlapping muffin-tin (MT) spheres and the interstitial region (IR). The basis functions $\phi_j(\mathbf{k}, \mathbf{R})$, where $j = 1, 2, ..., N_b$, are given by

$$\phi_j(\mathbf{k}, \mathbf{R}) = \begin{cases} v^{-1/2} \exp(i(\mathbf{k} + \mathbf{K}_j)\mathbf{R}), & \mathbf{R} \in IR, \\ \sum_{l,m} \mathcal{R}^{j,\alpha}_{l,m}(r, E_l)\, Y_{l,m}(\hat{r}), & \mathbf{R} \in MT(\alpha), \end{cases}$$

where $\mathbf{K}_j$ refers to the reciprocal lattice vector j, v is the unit cell volume, $Y_{l,m}$ are spherical harmonics [25] and the radial part is given by

$$\mathcal{R}^{j,\alpha}_{l,m}(r,\, E_l) = A^{j,\alpha}_{l,m}\, u_l(r, E_l) + B^{j,\alpha}_{l,m}\, \dot{u}_l(r, E_l). \qquad (1)$$

Here the index α refers to the type of atom (or MT-sphere) in the unit cell, the radius r is counted from the center $\mathbf{R}_\alpha$ of the sphere α (i. e., $\mathbf{r} = \mathbf{R} - \mathbf{R}_\alpha$). Radial functions $u_l(r, E_l)$ are solutions in the spherically averaged crystal potential computed at the linearization energy E_l, and $\dot{u}_l(r, E_l)$ is the derivative of u_l with respect to E at E_l. The coefficients $A^{j,\alpha}_{l,m}$ and

$B^{j,\alpha}_{l,m}$ are found from the condition that the basis function ϕ_j is continuous with continuous derivative at the sphere boundary, i. e., at $r = R^{\alpha}_{MT}$ (R^{α}_{MT} is the radius of the MT-sphere α). The coefficients $A^{j,\alpha}_{l,m}$ and $B^{j,\alpha}_{l,m}$ in Eq. (1) are related to the standard LAPW quantities a^j_l, b^j_l, expressed only through the spherical Bessel functions j_l and the radial solution u_l (and its derivatives) at $r = R^{\alpha}_{MT}$.

2.1. Explicitly averaged radial basis wave functions

Initially, the functions $u_l(r, E_l)$ in Eq. (1) were considered as the solutions of the Schrödinger equation in the spherically symmetric ($L = 0$) component of the total potential. Later, it appeared that some relativistic effects can be included in the so called scalar relativistic approach [19, 20]. Below we discuss the canonical radial functions introduced by Koelling and Harmon in [19], later justified by the procedure described by MacDonald, Pickett and Koelling in Ref. [20], and compare them with new radial functions that are more closely related to the Dirac solutions.

The standard LAPW radial basis functions are defined by an average

$$P^{av}_l(r) = \frac{l}{2l+1} P_l(r) + \frac{l+1}{2l+1} P_{-l-1}(r), \qquad (2)$$

where r is radius and P_l, P_{-l-1} are the large (L) components of the Dirac solutions P_{κ^L} for $\kappa^L = l$ ($j = l - 1/2$), and $\kappa^L = -l - 1$ ($j = l + 1/2$), correspondingly. (Here κ^L stands for the index κ of 2-spinors for the large component [26].) However, in practice the large components P_l and P_{-l-1} are not calculated. In Ref. [20] assuming that

$$\frac{d}{dr}(\delta P(r)) = \frac{d}{dr}\left(P_{-l-1}(r) - P_l(r)\right) = 0, \qquad (3)$$

an effective system for two coupled differential equations was derived. Then the LAPW radial basis function is

$$P^{KH}_l(r) = P^{av}_l(r)|_{\delta P'(r)=0}\,, \qquad (4)$$

i. e., the function (2), provided that the condition (3) is fulfilled. The second auxiliary function is an averaged small component $Q^{KH}_l(r)$ [20], given by Eq. (3b) of [20], but except in the system of differential equations, it is not used. As a result, P^{KH}_l, Q^{KH}_l depend only on l and include some relativistic effects. Although this approach has proved being efficient and practical, it has serious drawbacks when applied to heavy elements. In particular, Eq. (3) is an uncontrolled approximation,

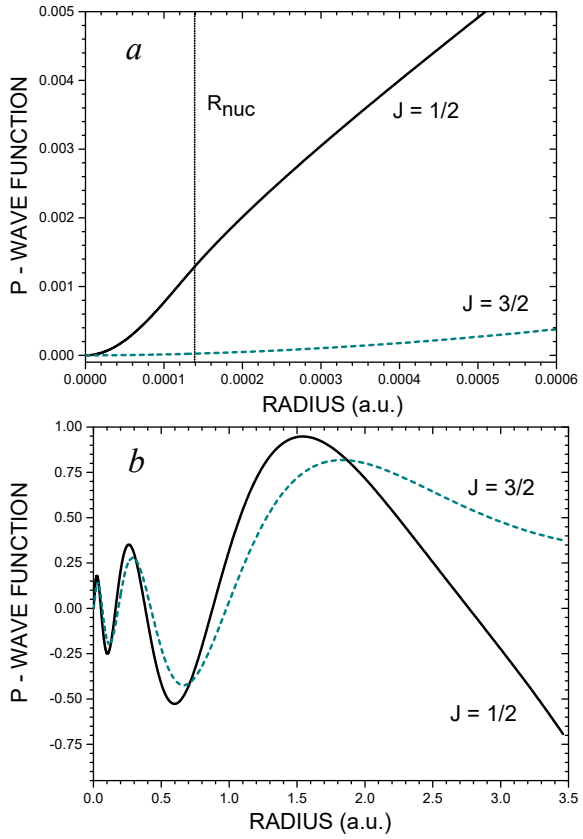

Fig. 1. Radial Dirac functions $P_{j=1/2}(r)$ and $P_{j=3/2}(r)$ of the $6p_{1/2}$ and $6p_{3/2}$ semicore states of actinium, (*a*) close to the nuclear region, and (*b*) inside the MT-sphere

and the averaging for Q^{KH}_l in Eq. (4) is a formal procedure, for angular two-spinors $\xi_{-\kappa,m}$, associated with the Dirac small components Q_{-l} and Q_{l+1}, have different angular dependencies [26].

To make the consideration on the radial part more concrete we consider the case of the face centered cubic (fcc) lattice of elemental actinium (with the PBE exchange correlation functional [27]). The most noticeable difference in the radial behavior of two large components with the same ℓ is observed for the $6p_{1/2}$ and $6p_{3/2}$ valence (semicore) states ($\ell = 1$) and below we consider it in more detail. It is well known that for the point nuclear case the corresponding Dirac solutions for $|\kappa| = 1$m, that is, for $s_{1/2}$- and $p_{1/2}$-states, have a singularity at the origin, which is absent for the $p_{3/2}$ radial functions. For the finite nuclear case, which is realized in our LAPW version, the singularity disappears (for the $p_{1/2}$-state, e. g., one has $P_{j=1/2} \propto r^2$) but the large radial functions $P_{j=1/2}(r)$ and $P_{j=3/2}(r)$ look quite different. In Fig. 1 we plot them at the same energy $E_{\ell=1}$ by solving numerically two Dirac equations. One clearly sees the different shape of large compo-

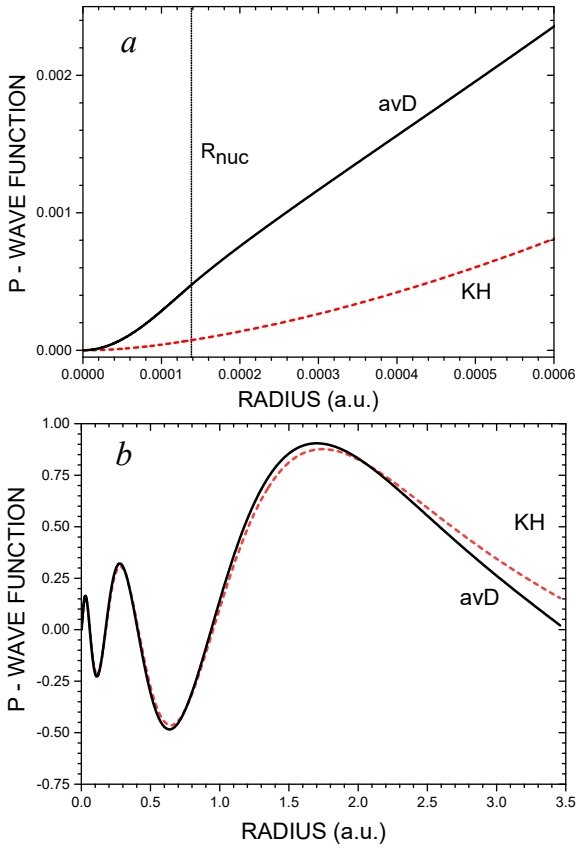

Fig. 2. Radial basis function $P^{av}_{\ell=1}(r)$ (avD) and the canonical KH radial basis function $P^{KH}_{l=1}(r)$ [19, 20] of the semicore $6p$-states of actinium, close to the nuclear region (*a*), and inside the MT-sphere (*b*)

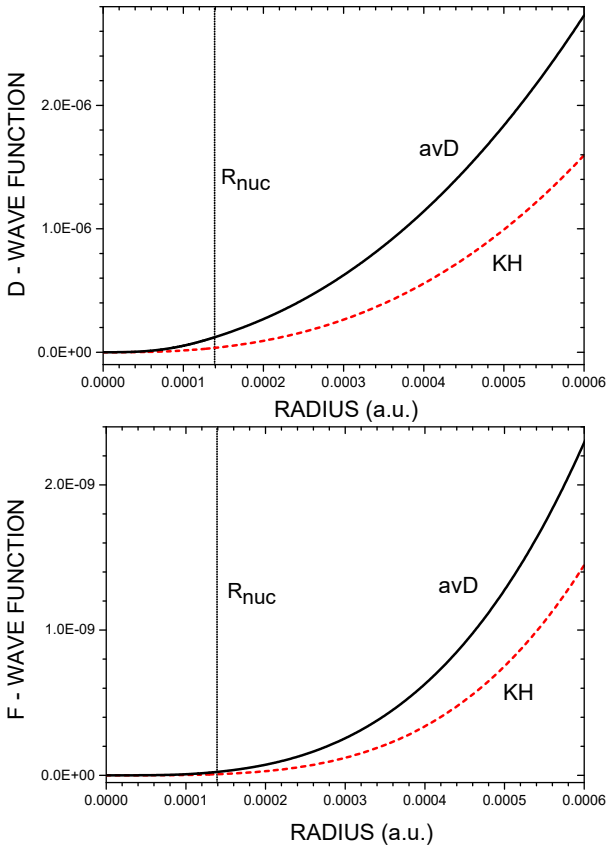

Fig. 3. Explicitly averaged radial functions $P^{av}_{\ell}(r)$ of Ac for $6d$ ($\ell = 2$) (*a*) and $5f$ ($\ell = 3$) (*b*) states and the corresponding canonical KH radial function $P^{KH}_{l}(r)$ [19, 20] close to the nuclear region

nents both at the large radii close to the MT-radius and at the neighborhood of the nuclear region. Then we calculate the average radial function $P^{av}_{\ell=1}(r)$ for the $6p$-states using Eq. (2) explicitly. This numerically averaged function $P^{av}_{\ell=1}(r)$, as well as the conventional LAPW function $P^{KH}_{l=1}$, obtained by solving the KH differential equations [19,20], are reproduced in Fig. 2. We see that the numerically averaged radial function $P^{av}_{\ell=1}$ remains different from $P^{KH}_{l=1}$ both at small and large radii, reflecting the approximate character of Eq. (3) and Eq. (4). In the following instead of $P^{KH}_{l=1}(r)$, and the corresponding energy derivative radial function

$$\dot{P}^{KH}_{\ell=1}(r) = \frac{\partial P^{KH}_{\ell=1}(r)}{\partial E},$$

required by the LAPW method, we suggest to use the explicitly averaged functions $P^{av}_{\ell=1}$, $\dot{P}^{av}_{\ell=1}$ as the $6p$ LAPW basis set. That is, we calculate first the Dirac functions P_l and P_{-l-1} ($l = 1$), after which we obtain the radial basis function P^{av}_{l} according to Eq. (2). A very important advantage of this scheme is that it avoids the use of the uncontrolled assumption (3).

Another advantage of $P^{av}_{l=1}$ of the $6p$-states is that the weight of the $P_{1/2}$ large component in it increases significantly, compared to the weight of $P_{1/2}$ in the canonical function $P^{KH}_{l=1}$. This is clearly visible in Fig. 2 where $P^{av}_{l=1}(r)$ deviates toward $P_{1/2}(r)$ at small and large radii.

Similarly to the explicit procedure of averaging $p_{1/2}$ and $p_{3/2}$, described above, we can introduce new radial functions for d- and f- (and high ℓ) states by using Eq. (2) for the independently calculated $j = l - 1/2$ and $j = l + 1/2$ Dirac radial functions. In the following we will refer to these directly averaged radial functions P^{av}_{ℓ} (large components) of the Dirac solutions as new basis functions (denoted as the basis set avD) comparing their performance with the standard KH basis functions P^{KH}_{l} (the KH basis set). To characterize quantitatively the difference between P^{av}_{ℓ} and P^{KH}_{l} ($\dot{P}^{av}_{\ell}$ and $\dot{P}^{KH}_{l}$) for $\ell > 0$ we introduce the deviation quantities $\triangle P_l$ and $\triangle \dot{P}_l$, defined as

$$\triangle P_l = \sqrt{\int_0^{R_{MT}} dr (P_\ell^{av}(r) - P_l^{KH}(r))^2}, \qquad (5a)$$

$$\triangle \dot{P}_l = \sqrt{\int_0^{R_{MT}} dr (\dot{P}_\ell^{av}(r) - \dot{P}_l^{KH}(r))^2}. \qquad (5b)$$

Calculated values of $\triangle P_l$ and $\triangle \dot{P}_l$ for various elements and compounds are listed in Table 1. Note that the large component of $s_{1/2}$ functions in both treatments coincides, i. e.,

$$P_{\ell=0}^{av} = P_{l=0}^{KH}, \quad \dot{P}_{\ell=0}^{av} = \dot{P}_{l=0}^{KH}.$$

Inspection of Table 1 shows that the largest difference between two functions (more than 10% of its norm) is found for basis 6*p*-states of actinides. The differences between the *d*- and *f*-functions are of the order of only 10^{-3}, but one should have in mind that Eq. (5a) and Eq. (5b) are integral. As we will see in Sec. 2.3 even this small difference matters for the calculation of SO coupling constants ζ, because in atomic units

$$\zeta = \frac{1}{2c^2} \left\langle \frac{1}{r} \frac{dV}{dr} \right\rangle_{av} \sim \left\langle \frac{Z}{r^3} \right\rangle_{av}, \qquad (6)$$

where $V(r)$ is the Coulomb potential. Therefore in this case the neighborhood of the nucleus, where the differences are visible, Fig. 3, contributes with considerably larger weight than the other regions. In general, however, the explicitly averaged radial functions (avD) for $6d$ ($P_{\ell=2}^{av}$), $5f$ ($P_{\ell=3}^{av}$) and higher ℓ-states demonstrate a much more close correspondence with the KH-radial functions $P_{l=2}^{KH}$, $P_{l=3}^{KH}$, etc., because of weak presence of these functions in the nuclear region. We will return to this problem in Sec. 2.3 below. Differences between the avD and KH radial basis functions for light elements such as oxygen in ThO_2 or UO_2 are negligible, Table 1.

2.2. Correction of LAPW matrix elements

The use of relativistic basis functions requires a modification of some matrix elements which are valid only in the non-relativistic limit. In particular, the matrix elements of the $L = 0$ component of the potental, as written in Eq. (16a) and Eq. (16b) of Ref. [8] are exact only in the nonrelativistic limit. The existence of this limitation is due to the fact that in deriving the expressions for the matrix elements, the equality

$$R_{MT}^2 (\dot{u}_l(R_{MT})\, u_l'(R_{MT}) - \dot{u}_l'(R_{MT})\, u_l(R_{MT})) = 1 \qquad (7)$$

is used. (Here, as before, the energy derivative $\dot{u}(r) = \partial u(r)/\partial E$ is defined in Rydberg energy units.) Eq. (7), explicitly quoted in Ref. [8] as Eq. (4), is exact only for the radial component u_l of the Schrödinger equation in the spherically symmetric potential.

In general, the expression on the left hand side of Eq. (7) deviates from unity for the effective radial components P_ℓ^{av}, $\dot{P}_\ell^{av}$ and P_l^{KH}, $\dot{P}_l^{KH}$, described in Sec. 2.1, because they are obtained from the Dirac equation. To illustrate this, in Table 2 we reproduce the values of the deviation factor

$$F(l) = R_{MT}^2 (\dot{P}_l(R_{MT})\, P_l'(R_{MT}) - \dot{P}_l'(R_{MT})\, P_l(R_{MT})) - 1, \qquad (8)$$

for the avD and KH radial basis functions. For the non-relativistic (Schrödinger) functions we have $F(l) \equiv 0$. In practice, as shown in Table 2 we find $F(l) \neq 0$. The deviations are the largest ($F(p) = -0.13$) for the radial $6p$-functions in the avD-basis set. In the KH basis set $F(l)$ are smaller, reaching only the value $F(p) \approx 7{\cdot}10^{-4}$ for $6p$-states of Ac. However, even such deviations can lead to a sizeable inaccuracy in determination of the equilibrium lattice constants and bulk moduli, and should be avoided.

The inequality $F(l) \neq 0$ requires amendments to some expressions of the LAPW method. The corrections involve the precise determination of the a_l and b_l coefficients and the matrix elements for the spherically symmetric component of the potential. In particular, Eq. (10b) and Eq. (10d) of Ref. [8] should be replaced with

$$a_l^n = \frac{1}{\triangle} (j_l'(k_n R_{MT})\, \dot{P}_l - j_l(k_n R_{MT})\, \dot{P}_l'), \qquad (9a)$$

$$b_l^n = \frac{1}{\triangle} (j_l(k_n R_{MT})\, P_l' - j_l'(k_n R_{MT})\, P_l), \qquad (9b)$$

where

$$\triangle = R_{MT}^2 (\dot{P}_l\, P_l' - P_l\, \dot{P}_l') \neq 1. \qquad (10)$$

The value for γ^l given in Eq. (16b) of Ref. [8], should also be rewritten. In the notation of Ref. [8] the following symmetric form can be obtained

$$\gamma^l = \frac{1}{2} \Big\{ a_l(\mathbf{k}_n) b_l(\mathbf{k}_m) + a_l(\mathbf{k}_m) b_l(\mathbf{k}_n) + \frac{1}{R_{MT}^2} (j_l'(n) j_l(m) + j_l(n) j_l'(m)) \Big\}. \qquad (11)$$

Here the second part with the Bessel functions comes from the MT-sphere boundary integration of the kinetic energy performed for the symmetrization of the expression for the matrix elements of kinetic energy, i. e., it appears due to the replacement of $\mathbf{k}_n \mathbf{k}_n U$ (or $\mathbf{k}_m \mathbf{k}_m U$) with $\mathbf{k}_n \mathbf{k}_m U$, Eq. (16a) of [8].

Table 1. Deviations $\triangle P_l$ and $\triangle \dot{P}_l$, Eq. (5a) and Eq. (5b), between two radial basis functions: the canonical (KH) P_l^{KH} ($\dot{P}_l^{KH}$) and the explicitly averaged Dirac (avD) functions P_ℓ^{av} ($\dot{P}_\ell^{av}$), Eq. (2), in fcc Th, fcc Ac, bcc Np, cubic ThO_2 [Th(2), O(2)] and UO_2 [O(3)] for $l > 0$; s-functions coincide ($\triangle P_{l=0} < 10^{-10}$)

		p	d	f	$\ell > 3$
Th	$\triangle P_l$	0.108	$1.1 \cdot 10^{-3}$	$1.5 \cdot 10^{-3}$	$< 2.3 \cdot 10^{-8}$
Th	$\triangle \dot{P}_l$	0.148	$1.4 \cdot 10^{-3}$	$3.9 \cdot 10^{-3}$	$< 1.7 \cdot 10^{-8}$
Th(2)	$\triangle P_l$	0.033	$4.3 \cdot 10^{-4}$	$3.4 \cdot 10^{-4}$	$< 1.0 \cdot 10^{-7}$
Th(2)	$\triangle \dot{P}_l$	0.012	$3.2 \cdot 10^{-4}$	$2.8 \cdot 10^{-4}$	$< 4.2 \cdot 10^{-8}$
O(2)	$\triangle P_l$	$2.9 \cdot 10^{-6}$	$2.2 \cdot 10^{-9}$	$5.5 \cdot 10^{-10}$	$< 3.3 \cdot 10^{-10}$
O(2)	$\triangle \dot{P}_l$	$2.8 \cdot 10^{-6}$	$9.4 \cdot 10^{-10}$	$2.3 \cdot 10^{-10}$	$< 2.9 \cdot 10^{-10}$
U	$\triangle P_l$	0.040	$5.6 \cdot 10^{-4}$	$6.3 \cdot 10^{-4}$	$< 1.5 \cdot 10^{-7}$
U	$\triangle \dot{P}_l$	0.014	$3.3 \cdot 10^{-4}$	$4.7 \cdot 10^{-4}$	$< 5.9 \cdot 10^{-8}$
O(3)	$\triangle P_l$	$2.9 \cdot 10^{-6}$	$2.3 \cdot 10^{-9}$	$5.5 \cdot 10^{-10}$	$< 3.3 \cdot 10^{-10}$
O(3)	$\triangle \dot{P}_l$	$2.6 \cdot 10^{-6}$	$9.7 \cdot 10^{-10}$	$2.1 \cdot 10^{-10}$	$< 2.9 \cdot 10^{-10}$
Ac	$\triangle P_l$	0.094	$9.2 \cdot 10^{-4}$	$5.3 \cdot 10^{-4}$	$< 1.5 \cdot 10^{-8}$
Ac	$\triangle \dot{P}_l$	0.170	$1.2 \cdot 10^{-3}$	$1.5 \cdot 10^{-3}$	$< 1.2 \cdot 10^{-8}$
Np	$\triangle P_l$	0.081	$9.3 \cdot 10^{-4}$	$1.8 \cdot 10^{-3}$	$< 8.1 \cdot 10^{-8}$
Np	$\triangle \dot{P}_l$	0.038	$6.4 \cdot 10^{-4}$	$1.9 \cdot 10^{-3}$	$< 4.3 \cdot 10^{-8}$

Table 2. Deviation of the factors $F(l)$ from zero, Eq. (8), for the avD, Eq. (2), and the canonical KH [19, 20] basis functions in fcc Th, fcc Ac, bcc Np, cubic ThO_2 [Th(2), O(2)] and UO_2 [O(3)], underlying the importance of the corrections for LAPW matrix elements, Eqs. (9a), (9b) and Eq. (11)

	basis	s	p	d	f
Th	avD	$1.2 \cdot 10^{-4}$	-0.129	$4.0 \cdot 10^{-4}$	$1.8 \cdot 10^{-4}$
Th	KH	$1.1 \cdot 10^{-4}$	$2.0 \cdot 10^{-4}$	$7.9 \cdot 10^{-5}$	$1.4 \cdot 10^{-4}$
Th(2)	avD	$5.1 \cdot 10^{-4}$	$3.3 \cdot 10^{-3}$	$8.5 \cdot 10^{-4}$	$2.4 \cdot 10^{-4}$
Th(2)	KH	$5.1 \cdot 10^{-4}$	$2.4 \cdot 10^{-4}$	$2.1 \cdot 10^{-4}$	$2.1 \cdot 10^{-4}$
O(2)	avD	$6.7 \cdot 10^{-5}$	$7.3 \cdot 10^{-5}$	$1.1 \cdot 10^{-5}$	$< 1e^{-6}$
O(2)	KH	$6.6 \cdot 10^{-5}$	$7.1 \cdot 10^{-5}$	$1.4 \cdot 10^{-5}$	$1.3 \cdot 10^{-5}$
U	avD	$5.2 \cdot 10^{-4}$	$1.5 \cdot 10^{-3}$	$8.3 \cdot 10^{-4}$	$2.6 \cdot 10^{-4}$
U	KH	$5.2 \cdot 10^{-4}$	$2.6 \cdot 10^{-4}$	$2.1 \cdot 10^{-4}$	$2.9 \cdot 10^{-4}$
O(3)	avD	$6.2 \cdot 10^{-5}$	$7.8 \cdot 10^{-5}$	$1.3 \cdot 10^{-5}$	$2.0 \cdot 10^{-6}$
O(3)	KH	$6.5 \cdot 10^{-5}$	$7.7 \cdot 10^{-5}$	$1.6 \cdot 10^{-5}$	$1.4 \cdot 10^{-5}$
Ac	avD	$1.0 \cdot 10^{-4}$	-0.126	$3.6 \cdot 10^{-4}$	$1.6 \cdot 10^{-4}$
Ac	KH	$7.5 \cdot 10^{-4}$	$6.8 \cdot 10^{-4}$	$4.5 \cdot 10^{-4}$	$3.9 \cdot 10^{-4}$
Np	avD	$2.6 \cdot 10^{-4}$	-0.039	$5.5 \cdot 10^{-4}$	$-2.9 \cdot 10^{-4}$
Np	KH	$2.6 \cdot 10^{-4}$	$2.4 \cdot 10^{-4}$	$1.3 \cdot 10^{-4}$	$3.1 \cdot 10^{-4}$

2.3. Calculated spin-orbit coupling constants, special treatment for 6*p*-states

In this section we consider how the new (avD) basis functions affect the values of the spin-orbit (SO) energy splittings. As a test exercise we first calculate spin-orbit coupling (SOC) constants and energy splittings for relativistic atoms of Ac, Th, U and Np with the PBE variant of DFT for exchange and correlations [27].

In atomic units the SO coupling constant $\zeta(l)$, defined by the radial function $P_l(r)$, can be found as

$$\zeta(l) = \frac{1}{2c^2} \int_0^\infty dr\, P_l^2(r)\, \frac{1}{r} \frac{dV}{dr}, \tag{12}$$

where $V(r)$ is the radial dependence of the Coulomb potential. The corresponding SO operator is

$$H^{SO} = \zeta(l)\, \hat{L}\hat{S}, \tag{13}$$

with energy splitting

$$\triangle_{SO}(l) = \zeta(l) \frac{2l+1}{2}. \tag{14}$$

As P_l we consider either P_ℓ^{av} (the avD basis) or P_l^{KH} (the KH basis). Comparing $\triangle_{SO}(l)$, Eq. (14), with the actual energy splitting $\triangle E(l)$, obtained by solving the Dirac atomic eigenproblem directly, we can conclude which basis set (avD or KH) gives a better description of the SO splitting. For the KH-basis, during the self-consistent procedure all core electron shells were obtained according to the fully relativistic Dirac approach whereas all valence electron shells according to the KH-equations [19,20], as is done in LAPW calculations. The calculated values of the SO coupling for $6d$-states are listed in Table 3, for $5f$-states in Table 4 and for $6p$-states in Table 5. Since for the avD-basis set we calculate individual Dirac radial components, we also quote the individual SO couplings $\zeta(l)$ for them, i. e., for $d_{3/2}$-, $d_{5/2}$-states in Table 3, for $f_{5/2}$-, $f_{7/2}$-states in Table 4 and for $p_{1/2}$-, $p_{3/2}$-states in Table 5.

Comparing $\triangle_{SO}(l)$ with $\triangle E(l)$ in Table 3 for d-states and Table 4 for f-states shows that in all cases the calculated SOC constants $\zeta^{avD}(\ell)$, based on P_ℓ^{av}-functions, give much better energy differences $\triangle_{SO}^{avD}(d)$, $\triangle_{SO}^{avD}(f)$ than $\triangle_{SO}^{KH}(d)$, $\triangle_{SO}^{KH}(f)$, based on the KH functions P_l^{KH}. This is directly related to the behavior of the avD and KH radial functions close to the nuclear region, where the functions $P_{\ell=2}^{av}$ ($P_{\ell=3}^{av}$) are systematically larger than $P_{l=2}^{KH}$ ($P_{l=3}^{KH}$), Fig. 3. Although the difference between the d and f basis functions in the whole region is rather small, Table 1, the larger values of $P_{\ell=2}^{av}$ ($P_{\ell=3}^{av}$) is the decisive factor which finally leads to larger SO coupling constants and better values for the energy splittings.

The situation however is changed for the SO interactions of $6p$-states. The reason for this is a very different radial dependence of the $p_{1/2}$ and $p_{3/2}$ radial components in the nuclear region, shown in Fig. 1 and Fig. 2, and discussed earlier in Sec 2.1. In the neighborhood of the nucleus, important for SOC, the $p_{1/2}$ component is very large (even singular for the point nucleus), and as a result, $\zeta_{1/2}$ calculated with the $p_{1/2}$ function is more than six times larger than $\zeta_{3/2}$ calculated with the $p_{3/2}$ component, Table 5. Even after the averaging between two p-components according to Eq. (2), the calculated SOC constant $\zeta^{avD}(p)$ overestimates approximately twice the actual SO-splitting, i. e., for the avD-basis $\triangle_{SO}(p) \approx 2 \times \triangle E(p)$, where $\triangle E(p) = E(6p_{3/2}) - E(6p_{1/2})$ is the actual splitting. The use of KH $6p$ radial functions improves the situation but it is also far from being ideal. Although in the nuclear region the KH-radial $6p$ functions $P_{l=1}^{KH}$ [19,20] is appreciably smaller than the corresponding avD-function $P_{\ell=1}^{av}$, Fig. 2 *a*, its SOC constant $\zeta^{KH}(p)$ remains large. Inspection of Table 5 shows that $\triangle_{SO}^{KH}(p)$ overestimates the actual values $\triangle E(p)$ by 17% for Ac, 19% for Th and 27% for Np. Earlier the problem of overestimated SO coupling effects was noticed, e. g., in Ref. [6]. The situation is aggravated by large absolute values of the $6p$-splittings (6.7–9.5 eV), which have a large impact on the band structure calculations.

From the Table 5 we can conclude that the actual energy splittings $\triangle E(p)$ between the $p_{1/2}$ and $p_{3/2}$-states are better approximated by the SO coupling constant $\zeta(p_{3/2})$ calculated using a single radial component $p_{3/2}$, for which $\triangle_{SO}^{*}(p) = 3\zeta(p_{3/2})/2$. For example, for Ac we obtain $\triangle_{SO}^{*}(p) = 6.09$ eV, for Th $\triangle_{SO}^{*}(p) = 7.12$ eV etc. Although the values $\triangle_{SO}^{*}(p)$ are slightly smaller than the real energy differences $\triangle E(p)$, they approximate $\triangle E(p)$ better (i. e., $9-11\%$ vs $17-27\%$) than the KH radial functions $P_{l=1}^{KH}$. The

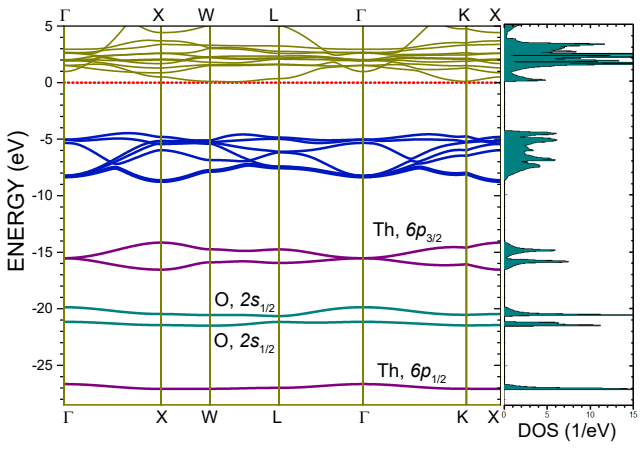

Fig. 4. Band structure of ThO_2 with the full SO coupling (left) and the density of electron states (DOS, right) in the KH radial function basis [19, 20]. The semicore $6p_{1/2}$- and $6p_{3/2}$-bands of Th (purple lines) are split by the SOC. The middle-point difference (11.5 eV) exceeds the $6p$ splitting in the Th atom (7.8 eV), see text for details

Table 3. Calculated SOC constants ζ (in eV) with the $6d_{3/2}$ and $6d_{5/2}$ radial functions in atoms. $\zeta(d)$ is the averaged value for two basis sets: avD, Eq. (2), and KH [19, 20]. $\triangle_{SO}(d)$ (in eV) is the corresponding SO energy splitting, whereas $\triangle E = E(6d_{5/2}) - E(6d_{3/2})$ (in eV) is the difference according to the fully relativistic Dirac atomic calculation

	Basis	$\zeta(d_{3/2})$	$\zeta(d_{5/2})$	$\zeta(d)$	$\triangle_{SO}(d)$	$\triangle E(d)$
Ac	avD	0.182	0.142	0.158	0.394	0.372
Ac	KH			0.125	0.313	0.372
Th	avD	0.250	0.196	0.216	0.541	0.510
Th	KH			0.182	0.456	0.510
U	avD	0.292	0.224	0.250	0.624	0.587
U	KH			0.212	0.531	0.587
Np	avD	0.254	0.188	0.214	0.534	0.502
Np	KH			0.230	0.574	0.502

Table 4. Calculated SOC constants ζ (in eV) with the $5f_{5/2}$ and $5f_{7/2}$ radial functions in atoms. $\zeta(f)$ is the averaged value for two basis sets: avD, Eq. (2), and KH [19, 20]. $\triangle_{SO}(f)$ (in eV) is the corresponding SO energy splitting, whereas $\triangle E = E(5f_{5/2}) - E(5f_{7/2})$ (in eV) is the difference according to the fully relativistic Dirac atomic calculation

	Basis	$\zeta(f_{5/2})$	$\zeta(f_{7/2})$	$\zeta(f)$	$\triangle_{SO}(f)$	$\triangle E(f)$
Th	avD	0.198	0.180	0.188	0.658	0.650
Th	KH			0.164	0.573	0.650
U	avD	0.276	0.254	0.263	0.922	0.909
U	KH			0.242	0.848	0.909
Np	avD	0.292	0.264	0.276	0.967	0.953
Np	KH			0.283	0.992	0.953

overestimation holds also for the solid case. Our data indicate that, for example, in ThO_2 for the canonical (KH) variant the SO splitting between the $6p$-subband midpoints is 11.5 eV (with the minimum and maximum difference being 10.1 and 12.9 eV) whereas in the atomic case it is only 7.8 eV, Fig. 4. Note that in the solid or atomic case the effective potential in the nuclear region, which mostly affects the splitting, is basically unchanged. Therefore, in the following for a more realistic description of the SO splittings for the $6p$ semicore band states within the LAPW method we suggest to use only $p_{3/2}$ radial component. Since the actual equations for the SO coupling in LAPW (see, e. g., Eq. (2) in [28]) differ from Eq. (12) and Eq. (13), and require three SO coupling constants $\zeta(p)$, $\dot{\zeta}(p)$, $\ddot{\zeta}(p)$, computed with two functions $P_{l=1}$ and $\dot{P}_{l=1}$, this implies that for their calculations we use $P_{3/2}$ (the $6p_{3/2}$ large component) and $\dot{P}_{3/2}$, which is the first energy derivative of the $6p_{3/2}$ large component.

For the other SOC calculations (that is, for the d and f and higher ℓ valence states) we use the standard procedure with the averaged radial components P_l^{av} and $\dot{P}_l^{av}$, Eq. (2), because, as discussed above, they give good approximations of the energy splittings in the atomic case (i. e., $\triangle_{SO}(d)$ and $\triangle_{SO}(f)$). Our results obtained using this SO treatment are presented in the Tables 6–9 below as avD variants. The KH variants in the Tables correspond to the canonical SO treatment, which as discussed earlier overestimates the $6p$ energy splitting. Here it is worth mentioning that the effect of overestimation of the $6p$ SO energy splitting is clearly visible in the full treatment of SOC (in the full basis set). The SOC calculated in the second variation step as a consequence of smaller basis set, gives smaller energies of the $6p$ splitting which can compensate this effect. Although in this Section we have considered the results with the PBE variant of DFT, the same conclusions can be drawn for other DFT functionals.

In addition to the SO couplings occurring inside the MT-sphere region, we have examined the SO effect in the interstitial region (IR). The matrix elements of the SOC there are given by

$$\langle \phi_p | V^{SO} | \phi_j \rangle = \frac{i}{4c^2} \sum_{\mathbf{K}} F(\mathbf{K}_j - \mathbf{K}_p + \mathbf{K})\, V_{\mathbf{K}} \times \times \left[\mathbf{K} \times (\mathbf{k} + \frac{1}{2}(\mathbf{K}_j + \mathbf{K}_p)) \right] \sigma, \quad (15)$$

where $\mathbf{K}_j$, $\mathbf{K}_p$ are the corresponding reciprocal lattice vectors, $V_{\mathbf{K}}$ is the Fourier component of the potential

Table 5. Calculated SOC constants ζ (in eV) with the $6p_{1/2}$ and $6p_{3/2}$ radial atomic functions. $\zeta(p)$ is the averaged value for two basis sets: avD, Eq. (2), and KH [19, 20]. $\triangle_{SO}$ (in eV) is the corresponding SO energy splitting, $\triangle^*_{SO} = \triangle_{SO}(p_{3/2})$ (in eV) is the energy splitting for $\zeta(p_{3/2})$, whereas $\triangle E = E(6p_{3/2}) - E(6p_{1/2})$ (in eV) is the actual difference according to the fully relativistic Dirac atomic calculation

	Basis	$\zeta(p_{1/2})$	$\zeta(p_{3/2})$	$\zeta(p)$	$\triangle^*_{SO}$	$\triangle_{SO}$	$\triangle E$
Ac	avD	26.22	4.06	8.17	6.09	12.25	6.69
Ac	KH			5.22		7.84	6.69
Th	avD	32.16	4.75	9.78	7.12	14.66	7.80
Th	KH			6.18		9.26	7.80
U	avD	42.98	5.58	12.28	8.36	18.42	9.26
U	KH			7.40		11.10	9.26
Np	avD	47.40	5.66	13.05	8.49	19.57	9.53
Np	KH			8.06		12.08	9.53

in IR, σ are the Pauli matrices, $F(\mathbf{K})$ are the standard LAPW integrals of $\exp(i\mathbf{KR})/v$ in IR. Our calculations indicate that the effect of the additional SOC in the interstitial region, Eq. (15), is negligible. This is related to the fact that the variations of the total potential in IR are very small in comparison with the changes near nuclei. Therefore, the interstitial region can be safely considered as nonrelativistic.

3. APPLICATION TO ACTINIDES

For calculation of the exchange-correlation potential and the exchange-correlation energy contribution within the DFT approach, we have used (1) the Perdew – Burke – Ernzerhof (PBE) scheme [27] of the generalized-gradient approximation (GGA), (2) PBEsol [29] which is a variant of PBE, and (3) the local density approximation (LDA) with the standard ($V_{exc} \propto -\rho^{1/3}$) exchange [30] and the PW-correlation [31]. For the band structure calculations we have used the Moscow-FLAPW program code [11, 28] which has been widely used by us before for the study of chemical bonding elemental solids and compounds. The technical parameters of numerical calculations are given in Appendix.

The results of our calculations are listed in Table 6 for fcc Ac, Table 7 for fcc Th, Table 8 for cubic ThO_2, and Table 9 for cubic UO_2. ThO_2 and UO_2 are crystallized in the CaF_2 structure. As discussed in the Introduction, first calculations of actinides [2, 4] and their oxides [3, 5, 32, 33] have been performed with the full potential LMTO method. Although nowadays the full potential LAPW (FLAPW) study of actinides [6,7] and dioxides [34, 35] are also available, the new feature of the present FLAPW calculations is the complete (full) treatment of the SO couplings, which effectively doubles the dimension of the basis set. This option makes difference with other FLAPW calculations of actinides [6, 7] where the SO coupling was incorporated at the second variational level [21, 22], which introduces certain uncontrolled approximations [10]. Recently, high precision PBE calculations of actinides and their oxides without SO coupling were reported in Ref. [36]. They can be compared with our results for the PBE variant with the canonical (KH) calculation without SOC. Our equilibrium lattice constants for Ac and Th agree with those given in the Supplementary information of [36] within 0.2% and 0.3%, respectively, while for the dioxides (ThO_2, UO_2), the difference is 1.2%. This discrepancy is explained by the use of different technical parameters (MT radii, etc.), local orbitals [11], and even fitting functions (we use the Murnaghan equation of state).

When comparing theoretical and experimental values of a and B, it should be taken into account that they are obtained under different conditions: the calculated values of a refer to zero temperature, and B to isothermal values, while the experimental values of a and B refer, respectively, to normal conditions and the adiabatic value. It is also worth mentioning that there are several theoretical studies of UO_2 with correlation effects (Hubbard repulsion) [12, 37–39, 41–43]. Such an approach however lies beyond the scope of the present work, which focuses on the peculiarities of the inclusion of relativistic effects.

All calculations in the present work are performed for two various basis sets (with the canonical (KH) radial functions and averaged Dirac [avD] functions, Sec. 2.1). For the avD basis sets we have used the corrected values for a^n_l, b^n_l, Eq. (9a), Eq. (9b), and Eq. (11)

Table 6. Results of LAPW calculations for fcc structure of elemental actinium (Ac) with the averaged Dirac (avD) and Koelling – Harmon [19] radial basis functions, with SOC (marked by $*$) and without it. a is the equilibrium lattice constant (in Å), B is the bulk modulus (in GPa). Experimental data: $a = 5.315$ Å [44], estimated $B = 24.5$ GPa [45]

DFT	Basis	SO	a (Å)	B, GPa
LDA	avD		5.576	28.2
LDA	avD	$*$	5.540	27.6
LDA	KH		5.496	31.5
LDA	KH	$*$	5.429	27.2
PBE	avD		5.756	24.6
PBE	avD	$*$	5.723	24.1
PBE	KH		5.682	24.6
PBE	KH	$*$	5.611	25.9
PBEsol	avD		5.633	25.9
PBEsol	avD	$*$	5.592	25.4
PBEsol	KH		5.553	26.0
PBEsol	KH	$*$	5.479	27.9

Table 7. Results of LAPW calculations for fcc structure of elemental thorium (Th) with the averaged Dirac (avD) and Koelling – Harmon [19] radial basis functions, with SOC (marked by $*$) and without it. a is the equilibrium lattice constant (in Å), B is the bulk modulus (in GPa). Experimental data: $a = 5.0845$ Å, $B = 58$ GPa [46]

DFT	Basis	SO	a (Å)	B, GPa
LDA	avD		5.015	74.1
LDA	avD	$*$	4.996	63.7
LDA	KH		4.956	82.7
LDA	KH	$*$	4.910	87.7
PBE	avD		5.142	57.0
PBE	avD	$*$	5.119	55.6
PBE	KH		5.066	57.7
PBE	KH	$*$	5.009	63.0
PBEsol	avD		5.054	58.6
PBEsol	avD	$*$	5.026	60.1
PBEsol	KH		4.971	61.7
PBEsol	KH	$*$	4.921	69.2

for γ^l for the matrix elements in the spherical ($L = 0$) component. For the KH basis set we have adopted the values given in Eq. (16a) and Eq. (16b) of Ref. [8]. In addition, we have carried out calculations with and without the SO coupling. For the calculation of the SO coupling constant of the $6p$ semicore states in the avD bases we used the $6p_{3/2}$ large component as described in Sec. 2.3, and for the KH basis the canonical averaged radial $6p$ component, which overestimates the SO energy splitting, see more details in Sec. 2.3. For the SO coupling constants of other valence states (i. e., d-, f-, and higher ℓ-states), we employed averaged radial functions, which, however, differ in the avD and KH schemes, Sec. 2.3.

Inspection of Tables 6–9 shows that even within the same DFT functional (LDA, PBE or PBEsol), various inclusions of relativistic effects lead to very different results for the equilibrium lattice constants and bulk modulii. In particular, the largest variation of a reaches 0.147 Å for fcc Ac (LDA) although in the case of ThO_2 it is only 0.019 Å for LDA and 0.01 Å for PBE and PBEsol. The largest difference in B reaches 26.2 GPa for fcc Th (LDA) and 24 GPa for UO_2 (LDA), although, for example, for Ac (PBE) it is only 2.4 GPa. Inclusion of the SO coupling leads to smaller lattice constants for fcc Ac and Th, but to larger ones for UO_2. As a rule, the SO coupling results in larger bulk moduli, but in some cases they practically do not change (Ac, PBE and PBEsol; ThO_2, all DFT) or even get smaller (Ac, LDA, PBE, PBEsol with avD; or UO_2 with all DFT variants).

The opposing trends are also found for the avD and KH basis sets. In some cases the use of the KH functions leads to smaller lattice constants (fcc Ac and Th), but in other instances (ThO_2 or UO_2) it gives larger values of a. The bulk moduli calculated with the KH functions can be larger (Th, all DFT variants; ThO_2, LDA), but also smaller than B found with the avD variants (UO_2, all DFT functionals). The other characteristics of the band structure are also susceptible to different treatment of relativistic effects. For example, the gap E_g of forbidden states in ThO_2 changes by 0.25 eV ($\sim 5\%$), Table 8.

It is also worth mentioning that in contrast to Th, our DFT calculations of the fcc structure of Ac appreciably overestimate its lattice constant even for LDA. This however was also noticed, e. g., in Ref. [48] ($a = 5.503$ Å in LDA) and very recently was also confirmed for the PBE LAPW variant without SOC [36] ($a = 5.669$ Å). Therefore, the effect should be attributed to the peculiarity of the band structure of this element. Our calculations indicate that this feature becomes more pronounced with increasing quality of the basis set. For example, decreasing the non-spherical components of electron density to $L_{max} = 6$ in the avD basis leads to a smaller lattice constants: 5.536 Å

Table 8. Results of LAPW calculations of uranium dioxide ThO_2 (CaF_2 structure) with with the averaged Dirac (avD) and Koelling – Harmon [19] radial basis functions, with SOC (marked by $*$) and without it. a is the equilibrium lattice constant (in Å), B is the bulk modulus (in GPa). Experimental data [47]: $a = 5.6001$ Å, $B = 198$ GPa

DFT	Basis	SO	a (Å)	B, GPa	E_g, eV
LDA	avD		5.587	201.0	4.65
LDA	avD	$*$	5.592	208.6	4.54
LDA	KH		5.596	232.3	4.50
LDA	KH	$*$	5.603	228.5	4.38
PBE	avD		5.686	198.5	4.69
PBE	avD	$*$	5.687	200.0	4.59
PBE	KH		5.692	198.4	4.53
PBE	KH	$*$	5.697	195.8	4.44
PBEsol	avD		5.621	215.3	4.63
PBEsol	avD	$*$	5.622	216.7	4.53
PBEsol	KH		5.627	215.4	4.50
PBEsol	KH	$*$	5.632	211.8	4.39

Table 9. Results of LAPW calculations of uranium dioxide UO_2 (CaF_2 structure) with with the averaged Dirac (avD) and Koelling – Harmon [19] radial basis functions, with SOC (marked by $*$) and without it. a is the equilibrium lattice constant (in Å), B is the bulk modulus (in GPa). Experimental data [47]: $a = 5.4731$ Å, $B = 207$ GPa

DFT	Basis	SO	a (Å)	B, GPa
LDA	avD		5.317	279.7
LDA	avD	$*$	5.346	264.5
LDA	KH		5.332	275.6
LDA	KH	$*$	5.358	255.7
PBE	avD		5.435	234.8
PBE	avD	$*$	5.468	224.3
PBE	KH		5.451	231.0
PBE	KH	$*$	5.481	216.8
PBEsol	avD		5.365	259.8
PBEsol	avD	$*$	5.396	245.1
PBEsol	KH		5.381	255.4
PBEsol	KH	$*$	5.408	237.3

($\delta a = -0.037$ Å) in LDA, 5.736 Å (-0.018 Å) in PBE, 5.597 Å (-0.032 Å) in PBEsol. Further, decrease of the basis set to only 65 functions results in 5.500 Å (total $\delta a = -0.073$ Å in LDA) 5.608 Å (-0.146 Å) in PBE, 5.539 Å (-0.09 Å) in PBEsol, compare with Table 6. Possibly, some properties of the phonon spectrum and mean square displacements of atoms in solid Ac make the description using poor basis sets more adequate to the experimental data. Owing to its scarcity and radioactivity, the experimental bulk modulus of Ac is unknown. To the best of our knowledge in the literature there is only an estimated (not directly measured) value of 24.5 GPa, listed in Ref. [45]. Theoretical bulk moduli are $B = 25.9$ GPa, obtained on the basis of a tight-binding (LDA) analysis [48], and $B = 23.9$ GPa in the canonical PBE LAPW variant without SOC [36]. All these values are in good correspondence with our data, Table 6.

Finally, we would like to comment on our calculations of UO_2, Table 9 and Fig. 5. In particular, it is often stated that in contrast to the experimental observations the plain band structure analysis predicts the metal character of this compound. This is not completely correct if the full SOC is taken into account. As shown in Fig. 5, when the full SO coupling is included, at the Fermi energy there is a small gap of 0.2–0.4 eV between the highest occupied and the lowest unoccupied $5f$ bands for any chosen **k**-vector. The appearance of the gap in the $5f$ band spectrum can be understood as follows. In the U atom the $5f_{5/2}$ and $5f_{7/2}$ electron states are split by approximately 1 eV because of the SO interaction. In the UO_2 compound each U atom is surrounded by 8 oxygen neighbors, and the corresponding crystal electric field (CEF) causes additional energy splittings according to the schemes [49],

$$D_{J=5/2} \to \Gamma_7 + \Gamma_8,$$
$$D_{J=7/2} \to \Gamma_6 + \Gamma_7 + \Gamma_8.$$

In particular, the lowest $J = 5/2$ level is split into a doublet (Γ_7) and a quartet (Γ_8). (The $5f$ CEF splittings can be traced at the Γ point in Fig. 5.) A small overlap of $5f$-states of U provides the electron band formation, with the Γ_8 quartet giving rise to two lowest unoccupied $5f$ bands, but, as follows from Fig. 5, a small energy difference between the $5f$-states, originating from the split Γ_7 and Γ_8-states, is preserved. The gap is not clearly observed because the occupied (Γ_7) and unoccupied (Γ_8) $5f$ bands slightly overlap at different **k**-vectors. For example, as follows from Fig. 5 the energy of the Γ_7 band in the vicinity of the Γ point is higher than the energy of the first Γ_8 band in the vicinity of the X point. (In fact, we have performed two different calculations: with the Γ_7 band, completely occupied, as shown in Fig. 5, and with a tiny occupation of the first Γ_8 band at the X point [not shown], but

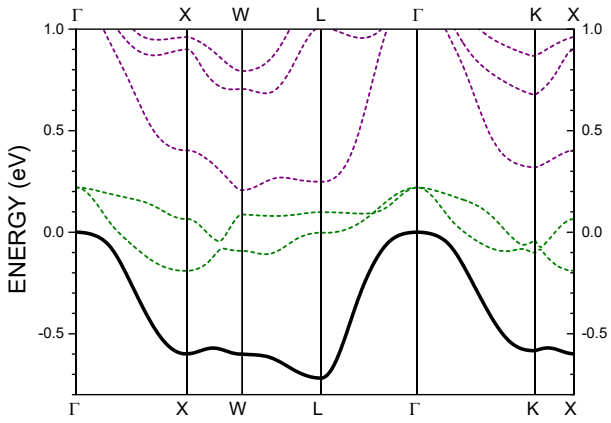

Fig. 5. The upper panel of the calculated band structure of UO_2 with the spin-orbit coupling, PBE calculation. The highest occupied $5f$ electron band is shown by solid line, lowest unoccupied $5f$ bands by dashed lines. The vertical gap with $\triangle E$ from 0.2–0.4 eV is visible. (The zero energy here corresponds to the position of the first $5f$ band at the Γ point, $E_F = -0.16$ eV)

the results were virtually the same.) Therefore, formally UO_2 should be classified as a semimetal.

It should be noted that, according to calculations presented in Ref. [50], crystalline germanium, which exhibits a small indirect band overlap, should also be classified as a semimetal. In reality, solid germanium is a semiconductor, and the semimetallic behavior is merely an artifact of the calculations. A similar correction could be applied to UO_2. In this case, according to experiment, it should be considered an insulator, while the semimetallic behavior is merely an artifact of the calculations.

4. CONCLUSIONS

Reviewing the treatment of relativistic effects in the LAPW method and avoiding using uncontrolled approximations, we have presented a new approach of dealing with the relativistic effects. First, we suggest to use new radial functions P_ℓ^{av} and $\dot{P}_\ell^{av}$ for the Bloch-type basis states. The functions are obtained by finding the large components $P_{\kappa=\ell}$, $P_{\kappa=-\ell-1}$ of the Dirac solutions independently for the $j = \ell - 1/2$ and $j = \ell + 1/2$-states at the same energy E_ℓ and then averaging them explicitly by means of Eq. (2). In applying this procedure to the $6p$ semicore states, we have found that the new scalar relativistic functions $P_{\ell=1}^{av}$ and $\dot{P}_{\ell=1}^{av}$ have more weight of the $6p_{1/2}$-states compared to the canonical basis functions $P_{\ell=1}^{KH}$ and $\dot{P}_{\ell=1}^{KH}$, and as a consequence, they can describe the $6p$ electron density without the $6p_{1/2}$ local atomic function as done in the LAPW+$p_{1/2}$ method. The functions P_ℓ^{av} and $\dot{P}_\ell^{av}$ can be further enriched with local atomic-like orbitals [11, 21–24] as done with the canonical (KH) basis set.

Second, we have corrected the LAPW expressions for a_l^n, b_l^n, Eq. (9a), Eq. (9b), and for the matrix elements in the spherical ($L = 0$) component of the total potential, using Eq. (11) for γ^l. The canonical expression for γ^l given in Eq. (16a) and Eq. (16b) of Ref. [8] implicitly uses Eq. (7), which is valid only for the non-relativistic radial solutions u_l and $\dot{u}_l$, Sec. 2.2.

Third, since in the full SO treatment the splitting between $6p_{1/2}$ and $6p_{3/2}$ bands is overestimated (see Fig. 4 and the discussion in Sec. 2.3), for the calculation of the SOC constants $\zeta(p)$, $\dot{\zeta}(p)$, $\ddot{\zeta}(p)$ for the semicore $6p$-states we have used the large component of the Dirac solution for the $6p_{3/2}$-states $P_{\kappa=-2}$ and its energy derivative $\dot{P}_{\kappa=-2}$, which gives better approximation for the actual energy splittings, Sec. 2.3. We stress that this treatment holds only for the $6p$-states. For $6d$, $5f$ and high ℓ levels, the SOC constants are calculated with the new *averaged* radial components P_ℓ^{av}, $\dot{P}_\ell^{av}$, because they describe the SO energy splittings adequately (i. e., for the high ℓ-states P_ℓ^{av}, $\dot{P}_\ell^{av}$ simply substitute the canonical radial functions P_ℓ^{KH}, $\dot{P}_\ell^{KH}$ in the LAPW expressions for SOC), Sec. 2.3.

Our calculations include the SO coupling for valence states in the full (doubled) basis space, which differs from other studies where the SO coupling is treated as a second variation step [10, 21, 22]. In addition, in the second variation step method relativistic effects are accounted for by adding relativistic local orbitals (like $6p_{1/2}$) to the LAPW basis set whereas in our approach they are included in the Bloch-like LAPW basis functions. The same type of radial functions (i. e., P_ℓ^{av}, $\dot{P}_\ell^{av}$) can be used for the construction of local orbital functions described in Ref. [11]. Therefore, our approach can be considered as an alternative to the description of relativistic effects within the second variation method.

Based on our study, we have found that the difference in the treatment of relativistic effects can result in uncertainties up to 0.15 Å for lattice constants and to 26 GPa for bulk moduli even within the same chosen DFT functional (LDA, PBE or PBEsol), Tables 6–9. Unfortunately, as discussed in Sec. 3 it is not possible to conclude on the direction of the changes (i. e., increase or decrease of a or B) when different relativistic treatments are involved: in different materials the trends are opposite.

The inclusion of the SO coupling in the interstitial region, using Eq. (15) for the matrix elements, turned out to be negligible.

It is worth noting that in the literature the band structure of UO_2, is often considered metallic. Although our study of UO_2 also indicates a small overlap at the Fermi energy, more close examination shows that the overlap is indirect, Fig. 5. The full treatment of the SO coupling clearly demonstrates the presence of a small gap ($\sim 0.2 - 0.4$ eV) at E_F, which is preserved for all **k**-vectors. Therefore, UO_2 is a semimetal.

We have also found that DFT calculations for the fcc structure of actinium significantly overestimate its lattice constant for all variants of the DFT functionals, Table 6. This effect becomes more pronounced with increasing basis set quality, Sec. 3. The best fit to the experimental value (with a difference of $\triangle a = 0.185$ Å) is achieved in LDA for a basis set of 65 basis functions with $L_{max} = 6$.

Acknowledgements. This research was supported by a grant of the Russian Science Foundation (Project No. 24-12-00053).

Conflict of interest. The authors declare that they have no conflicts of interest.

Authors' contributions. The contributions of the authors are equal.

APPENDIX. TECHNICAL PARAMETERS OF CALCULATIONS

For the band structure calculations we have used the Moscow-FLAPW program code [11, 28]. The technical parameters of numerical calculations were as follows. For fcc Ac and fcc Th, in most cases the number of augmented plane waves was 137 and 274 (with SO), with $R_{MT}K_j \sim 10$, where $\mathbf{K}_j$ is the maximal wave vector, and R_{MT} is the radius of the MT-sphere. For CaF_2 cubic structures, the basis sets were 307 and 614 (with SO) for ThO_2 ($R_{MT}K_j \sim 8.7$), 387 and 774 (with SO) for UO_2 ($R_{MT}K_j \sim 9.5$). For the canonical (KH) basis two sets of local $6p$-functions (u and $\dot{u}$) as described in Ref. [11]. Therefore, for the KH-calculations the total number of basis functions is 143 and 286 (with SO) for Ac and Th, 313 and 626 (with SO) for ThO_2, and 393 and 786 for UO_2. The following radii of MT-spheres have been used: for Ac 3.46 a.u. for all DFT functionals (i. e., LDA, PBEsol, PBE); for Th 3.05 a.u. (LDA), 3.12 a.u. (PBEsol and PBE); for ThO_2 2.25 a.u. for both Th and O for all DFT functionals; for UO_2 2.138 a.u. (LDA), 2.168 a.u. (PBEsol, PBE) for both U and O. It is worth noticing that within the chosen DFT functional we used the same R_{MT} for all variants of the different radial functions (i. e., avD, KH with and without SOC). The linear energy parameter $E_{\ell=1}$ for p-states was taken in the midpoint of the semicore $6p$ bands. The maximal number of k-points in the irreducible part (IP) of the Brillouin zone (BZ) for elemental actinides was 1505 ($\sim$ 70000 for the whole BZ). For ThO_2 and UO_2 we have used a set of 240 k-points in IP of BZ ($\sim$ 11500 for the whole BZ). The maximal value of the LAPW plane-wave expansion and the non-spherical density decomposition was $L_{max} = 8$. We have taken into account the finite size of nuclei and used the tetrahedron method for the linear interpolation of energy between k-points [51]. The number of radial points inside the MT sphere region was increased to 4000–4200 for actinides and 900–1000 for oxygen. The enlarged number of radial points is analogous to the increase of the quality of the basis set, and this is certainly required for the actinides with 80 core electrons, which is a very large quantity. The calculations with the KH basis sets have been performed with additional localized atomic p basis functions as described in Ref. [11]. We cannot perform the canonical (KH) calculations without supplying the basis set with local orbitals — such calculations are plagued with ghost states, or they crush and do not converge. In the case of new radial basis functions P_ℓ^{av} (avD) the calculations could proceed regularly until the convergence is reached. For that reason, all calculations marked in the Tables as avD (with and without SO) have been carried out without local functions.

REFERENCES

1. K. Lejaeghere et al., Science **351**, 1415 (2016).

2. P. Söderlind, Advances in Physics **47**, 959 (1998).

3. L. Petit, A. Svane, Z. Szotek, W. M. Temmerman, and G. M. Stocks, Phys. Rev. B **81**, 045108 (2010).

4. P. Söderlind, O. Eriksson, J. M. Wills, and A. M. Boring, Phys. Rev. B **48**, 9306 (1993).

5. S. Li, R. Ahuja, B. Johansson, High Pressure Research: Int. J. **22**, 471 (2002).

6. M. D. Jones, J. C. Boettger, R. C. Albers, and D. J. Singh, Phys. Rev. B **61**, 4644 (2000).

7. Pénicaud, J. Phys.: Condens. Matter **12**, 5819 (2000).

8. D. D. Koelling and G. O. Arbman, J. Phys. F: Metal Phys., **5**, 2041 (1975).

9. P. Blaha, K. Schwarz, G. Madsen, D. Kvasnicka, and J. Luitz, J. Luitz, WIEN2K: *An Augmented Plane Wave plus Local Orbitals Program for Calculating Crystal Properties*, Vienna University of Technology, Austria (2001).

10. D. J. Singh and L. Nordström, *Planewaves, Pseudopotentials, and the LAPW Method*, 2nd ed., Springer, New York (2006).

11. A. V. Nikolaev, D. Lamoen, and B. Partoens, J. Chem. Phys. **145**, 014101 (2016).

12. G. H. Lander, Science **301**, 1057 (2003).

13. H. L. Skriver, O. K. Andersen, and B. Johansson, Phys. Rev. Lett. **41**, 42 (1978).

14. J. L. Sarrao, L. A. Morales, J. D. Thompson, B. L. Scott, G. R. Stewart, F. Wastin, J. Rebizant, P. Boulet, E. Colineau, and G. H. Lander, Nature (London) **420**, 297 (2002).

15. S. Heathman, R. G. Haire, T. Le Bihan, A. Lindbaum, M. Idiri, P. Normile, S. Li, R. Ahuja, B. Johansson, and G. H. Lander, Science **309**, 110 (2005).

16. L. Petit, A. Svane, Z. Szotek, and W. M. Temmerman, Molecular Phys. Rep. **38**, 20 (2003); Science **301**, 498 (2003).

17. P. A. Korzhavyi, L. Vitos, D. A. Andersson, and B. Johansson, Nat. Mater. **3**, 225 (2004).

18. P. Söderlind, O. Eriksson, B. Johansson, J. M. Wills, and A. M. Boring, Nature (London) **374**, 524 (1995).

19. D. D. Koelling and B. N. Harmon, J. Phys. C: Solid State Phys., **10**, 3107 (1977).

20. A. H. MacDonald, W. E. Pickett, and D. D. Koelling, J. Phys. C: Solid St. Phys. **13**, 2675 (1980).

21. J. Kuneš, P. Novák, R. Schmid, P. Blaha, and K. Schwarz, Phys. Rev. B **64**, 153102 (2001).

22. C. Vona, S. Lubeck, H. Kleine, A. Gulans, and C. Draxl, Phys. Rev. B **108**, 235161 (2023).

23. G. Michalicek, M. Betzinger, C. Friedrich, and S. Blügel, Comput. Phys. Commun. **184**, 2670 (2013)

24. F. Karsai, F. Tran, and P. Blaha, Comput. Phys. Commun. **220**, 230 (2017).

25. C. J. Bradley and A. P. Cracknell, *The Mathematical Theory of Symmetry in Solids*, Clarendon, Oxford (1972).

26. K. G. Dyall and K. Fægri, Jr., *Introduction to Relativistic Quantum Chemistry*, Oxford, University Press (2007).

27. J. P. Perdew, K. Burke, and M. Ernzerhof, Phys. Rev. Lett. **77**, 3865 (1996); erratum: Phys. Rev. Lett. **78**, 1396 (1997).

28. A. V. Nikolaev, I. T. Zuraeva, G. V. Ionova, and B. V. Andreev, Fizika Tverdogo Tela **35**, 414 (1993). [Phys. Solid State **35**, 213 (1993)].

29. J. P. Perdew, A. Ruzsinszky, G. I. Csonka, O. A. Vydrov, G. E. Scuseria, L. A. Constantin, X. Zhou, and K. Burke, Phys. Rev. Lett. **100**, 136406 (2008); erratum: **102**, 039902 (2009).

30. P. A. M. Dirac, Proc. Camb. Philos. Soc. **26**, 376 (1930).

31. J. P. Perdew and Y. Wang, Phys. Rev. B **45**, 13244 (1992); erratum: Phys. Rev. B **98**, 079904 (2018).

32. J. Staun Olsen, L. Gerward, V. Kanchana, and G. Vaitheeswaran, J. Alloys and Compounds **381**, 37 (2004).

33. V. Kanchana, G. Vaitheeswaran, A. Svane, and A. Delin, J. Phys.: Condens. Matter **18**, 9615 (2006).

34. R. Terki, H. Feraoun, G. Bertrand, and H. Aourag, Comput. Mater. Sci. **33**, 44 (2005).

35. I. R. Shein, K. I. Shein, and A. L. Ivanovskii, J. Nuclear Mater. **361**, 69 (2007).

36. E. Bosoni, L. Beal, M. Bercx et al., Nat. Rev. Phys. **6**, 45 (2024).

37. I. D. Prodan, G. E. Scuseria, and R. L. Martin, Phys. Rev. B **76**, 033101 (2007).

38. H. Shi, M. Chu, and P. Zhang, J. Nuclear Mater. **400**, 151 (2010).

39. A. J. Devey, J. Nuclear Mater. **412**, 301 (2011).

40. B.-T. Wang, P. Zhang, R. Lizárraga, I. Di Marco, and O. Eriksson, Phys. Rev. B **88**, 104107 (2013).

41. E. Vathonne, J. Wiktor, M. Freyss, G. Jomard, and M. Bertolus, J. Phys.: Condens. Matter **26**, 325501 (2014).

42. P.-F. Sui, Z.-H. Dai, X.-L. Zhang, and Y.-C. Zhao, Chin. Phys. Lett. **32**, 077101 (2015).

43. F. Bruneval, M. Freyss, and J.-P. Crocombette, Phys. Rev. Mater. **2**, 023801 (2018).

44. J. W. Arblaster, *Selected Values of the Crystallographic Properties of the Elements. ASM International*, Materials Park, Ohio (2018).

45. K. A. Gschneidner, Jr., J. Phys. C: Solid St. Phys. **16**, 275 (1964).

46. G. Bellussi, U. Benedict, and W. B. Holzapfel, J. Less-Common Met. **78**, 147 (1981).

47. M. Idiri, T. Le Bihan, S. Heathman, and J. Rebizant, Phys. Rev. B **70**, 014113 (2004).

48. J. Durgavich, S. Sayed, and D. Papaconstantopoulos, Comput. Mater. Sci. **112**, 395 (2016).

49. M. Tinkham, *Group Theory and Quantum Mechanics*, McGraw-Hill, New York (1964).

50. R. Asahi, W. Mannstadt, and A. J. Freeman, Phys. Rev. B **59**, 7486 (1999).

51. G. Lehmann and M. Taut, Phys. St. Solid. B **54**, 469 (1972).